Design of a FSAE Cooling System

by

Harriet Alicia Chiu

Submitted to the
Department of Mechanical Engineering
in Partial Fulfillment of the Requirements for the Degree of

Bachelor of Science in Mechanical Engineering

at the

Massachusetts Institute of Technology

June 2019

Signature redacted

Signature of Author: _____
Department of Mechanical Engineering
May 16, 2019

Signature redacted

Certified by: _____
Irmgard Bischofberger
Assistant Professor of Mechanical Engineering
Thesis Supervisor

Signature redacted

Accepted by: _____
Maria Yang
Professor of Mechanical Engineering
Undergraduate Officer

Design of a FSAE Cooling System

by

Harriet Chiu

Submitted to the Department of Mechanical Engineering
on May 16, 2019 in Partial Fulfillment of the
Requirements for the Degree of

Bachelor of Science in Mechanical Engineering

ABSTRACT

MIT Motorsports is a FSAE Electric team at MIT that designs, manufactures, and tests electric formula-style racecars to compete in an annual collegiate competition. The cooling system for the Model Year 19 vehicle must provide adequate cooling to the motors and motor controllers, meet power consumption requirements dictated by the low voltage battery, and minimize system mass. Fluid modelling and benchtop testing were used to select the most suitable pump, fan and radiator. Tube routing and mounting design also have to allow for serviceability. With the use of a cooling test bench, a flow architecture was developed, and components were modified and tested to meet specifications.

Thesis Supervisor: Irmgard Bischofberger
Title: Assistant Professor of Mechanical Engineering

ACKNOWLEDGEMENTS

This thesis is dedicated to MIT Motorsports. Special thanks to Serena Grown-Haeberli for her leadership of team and moral support, Jeremy Noel for his help every step of the way, Ethan Perrin for the construction of the cooling bench, Asli Demir for her thermal and fluids wisdom and battery room shenanigans, Zoe Levitt for her help with running tests on cooling bench, Cheyenne Hua for her harnesses, Audrey Gaither for her help with assembly, and Alex Hattori for his help with frankenpump. I would also like to thank alumni of the team who have worked on the cooling system in the past, including Elliot Owen and Luis Mora.

Thanks to Irmgard Bischofberger for being a wonderful thesis advisor, and for her thoughtful comments on this paper.

Lastly, I would like to thank my family for their love and support.

TABLE OF CONTENTS

ABSTRACT 2
ACKNOWLEDGEMENTS 3
TABLE OF CONTENTS 4
LIST OF FIGURES 5
LIST OF TABLES 5
1. INTRODUCTION 6
1.1 FORMULA SAE AND MIT MOTORSPORTS 6
2. BACKGROUND 7
2.1 INTRODUCTION TO COOLING SYSTEM 7
2.2 SYSTEM REQUIREMENTS 8
3. DESIGN 9
3.1 SYSTEM INPUTS 9
3.2 COOLING SYSTEM EQUATIONS 10
3.3 PRESSURE DROP TESTING 10
3.4 ARCHITECTURE 12
3.5 COOLING COMPONENTS 13
PUMP 13
RADIATOR AND FAN 16
SWIRL POT 18
CAD 20
4. SYSTEM PERFORMANCE 21
5. CONCLUSIONS AND FUTURE WORK 22
APPENDIX 23
REFERENCES 24

LIST OF FIGURES

Figure 1: Force vs time graph for all-wheel drive 6

Figure 2: Powertrain architecture for MY19 7

Figure 3: Rinehart temperature data from MY18 endurance 8

Figures 4a and 4b: Emrax (a) and Hawk 40 (b) efficiency maps. 9

Figure 5: Block diagram of cooling test bench 11

Figure 6: Cooling test bench setup 11

Figure 7: Pressure drop of Rinehart, Emrax and Hawk 40 motors with varying flowrates 12

Figure 8: Parallel flow architecture 13

Figure 9: Everflo Diaphragm Pump Model EF7000 14

Figure 10: The prototype pump 15

Figure 11a and 11b: Frankenpump flowrate test setup and flowmeter 15

Figure 12: Total pressure drop across radiator 17

Figure 13: Fan curves with radiator pressure drop 17

Figure 14: Radiator and fan shroud assembly 18

Figure 15a and 15b: Swirl pot features 18

Figure 16: Solidworks Flow Simulation flow trajectory 19

Figure 17: CAD of cooling system 20

Figure 18: MY18 radiator and fan setup on the cooling test bench 21

Figure 19: Heat dissipation of various radiators and fans at different flowrates 22

LIST OF TABLES

Table 1: Component flowrate, water temperature and pressure limit requirements 9

Table 2: Minor loss coefficients 10

Table 3: Results from iterative flowrate-pressure drop calculation. 13

1. INTRODUCTION

1.1 FORMULA SAE AND MIT MOTORSPORTS

MIT Motorsports is a Formula SAE Electric team that competes in the Formula SAE collegiate competition annually. Teams design, manufacture, test and race a formula-style racecar, and are judged based on design, cost and track performance of the vehicle. The model year 17 (MY17) and model year 18 (MY18) vehicles of MIT Motorsports have the same architecture, with rear-wheel drive and a custom air-cooled battery pack. MY17 won second place overall at the 2017 competition, while MY18 achieved the fastest acceleration, autocross and endurance times at the 2018 competition.

With two model years of electrically and mechanically reliable rear-wheel drive vehicles, the team decided to take on the challenge of building our first all-wheel drive vehicle for MY19. This decision was informed by simulations that proved that adding front motors decreased acceleration time from 4.02 sec to 3.75 sec for a 306 kg car. This is because from a power perspective, an all-wheel drive car is limited by friction at the tires and the 80kW power limit on both front and rear wheels, as opposed to tractive power from the motors, as shown in Figure 1.

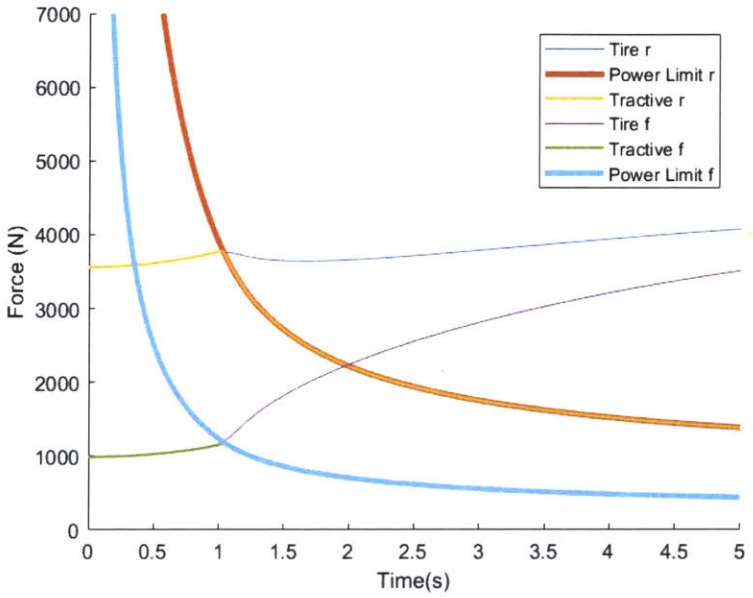

Figure 1: Force vs time graph of the resultant forces of the 3 sources of power at the front (f) and rear (r) wheels during acceleration – tire friction, tractive power and the 80kW power limit. In all-wheel drive, both front and rear powertrains are limited by friction of the tires, and then by the 80kW power limit imposed by FSAE rules.

Moving to all-wheel drive means that the cooling system has to cool more motors and motor controllers. A new flow architecture was determined through analytical modelling and empirical testing. On the component level, cooling components were tested for performance and optimized for mass.

2. BACKGROUND

2.1 INTRODUCTION TO COOLING SYSTEM

The cooling system on an electric formula-style vehicle water cools the motors and motor controllers. The rear powertrain on MY18 consists of the Emrax 228 motor, and the Rinehart PM100 motor controller.

On the MY19 vehicle, the rear powertrain maintains the same architecture with the Emrax and Rinehart. For the front powertrain, two Hawk 40 motors were selected and they would be paired with Bamocar D3 motor controllers, as shown in Figure 2. A custom enclosure was designed for the Bamocars, with custom cold plates that meet the heat dissipation requirements.

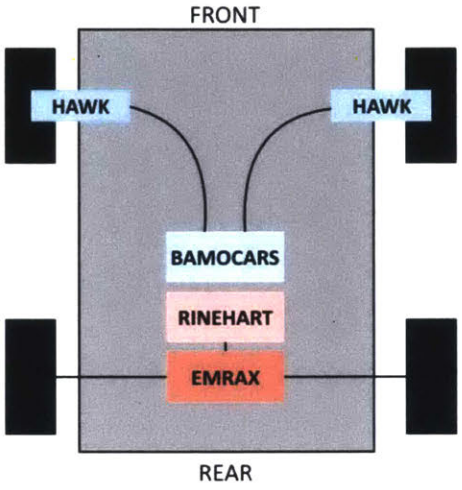

Figure 2: Powertrain architecture of MY19 showing the two Hawk motors in the front wheel packages, the Emrax motor in the rear. The Bamocar and Rinehart motor controllers are connected to the motors as shown.

2.2 SYSTEM REQUIREMENTS

The MY18 cooling system was able to adequately cool the Emrax and Rinehart. Rinehart temperature sensor data from the endurance event at competition showed that internal temperatures of the Rinehart peaked at 59.2°C, as seen in Figure 3. The maximum allowable temperature of 80°C was never exceeded.

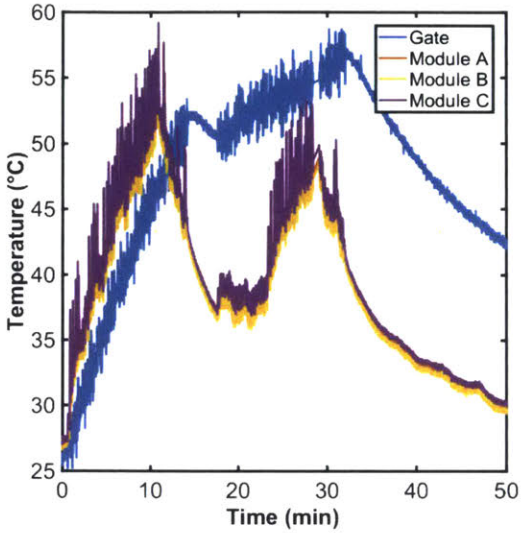

Figure 3: Rinehart temperature data from built-in sensors at the gate and at 3 points in the internal modules. The drops in temperature from minute 10 to 23 and from minute 30 onwards are due to limp mode, which limits power output so that our battery does not overheat.

The main issues with MY18's cooling system were identified to be:

1. Lack of optimization, resulting in heavy system mass. The 3.17 kg diaphragm pump contributed the majority of the cooling system mass.
2. Poor packaging of components meant that mounting of the swirl pot, pump and radiator and fan assembly were difficult to access.

MY19's cooling system seeks to improve upon MY18's and meet the system level requirements of:

1. Providing adequate cooling to the critical components
2. Operating reliably without leaks, contaminants or excessive air in the tubes
3. Designing a well packaged system and stiff mounting
4. Meeting power consumptions requirements
5. Limiting impact on aerodynamics of the vehicle
6. Following relevant rules of the FSAE competition (see appendix)

3. DESIGN

3.1 SYSTEM INPUTS

The motor and motor controller manufacturers provide guidelines that the components should operate at, as summarized in Table 1.

Table 1: Flowrate, water temperature and pressure limit requirements of the Rinehart, Emrax, Bamocar and Hawk 40 motors as specified by their respective manufacturers [1],[2],[3],[4]. The minimum flowrate across components is 7 to 8 LPM, and the maximum is 12 LPM.

	Minimum Flowrate [LPM]	Maximum Flowrate [LPM]	Maximum Water Temp [°C]	Pressure Limit [bar]
Rinehart	8	12	80	-
Emrax	7	-	50	2
Bamocar	-	-	65	-
Hawk 40	7.5	12	47	-

Motor and motor controller efficiencies were used to determine the required power dissipation of the cooling system. The Rinehart has a minimum efficiency of 97% ($e_{rinehart}$), the Emrax 92% (e_{emrax}),the Bamocars 92% (e_{bamo}), and the Hawks 92% (e_{hawk}).

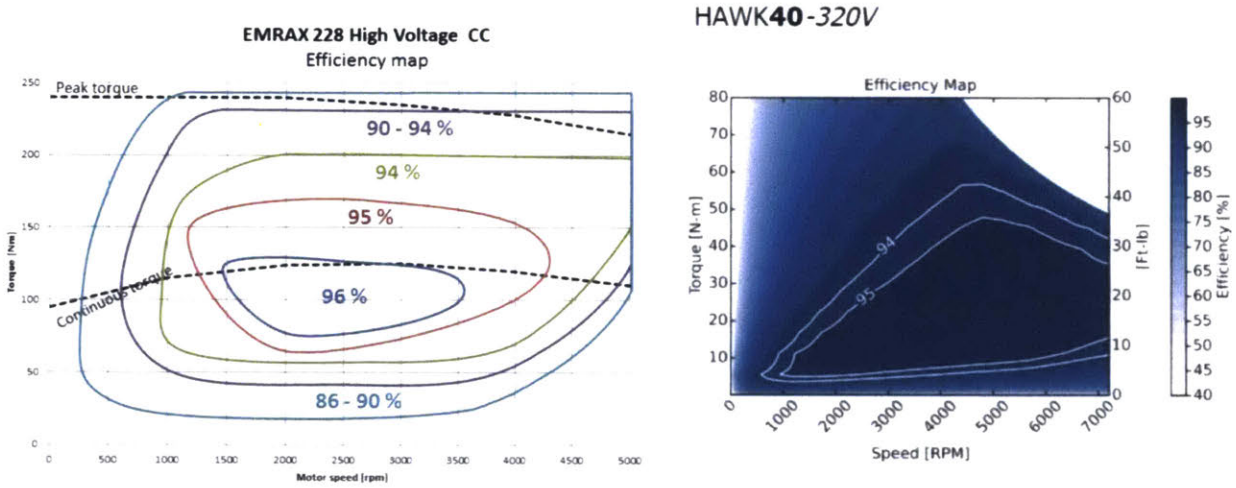

Figures 4a and 4b: Emrax (a) and Hawk 40 (b) efficiency maps. 92% efficiency for both components were chosen to be the worst case scenario given our operating points [2],[4].

MY18 had an average power draw of 30 kW, which meant that the cooling system dissipated 3.2 kW in its worst case. We estimate that MY19 would have a similar average power draw of 30kW. Through simulations that take into account tractive power, power from the tires and the power limit of 80kW, the optimal power split of 24.12% front (s_{front}) and 75.88% rear (s_{rear}) was determined. Using equations (1) and (2), the power from the inefficiencies in the front and rear powertrain can be calculated.

$$P_{dissipated,front} = 30kW \times s_{front} \times [(1 - e_{bamo}) + e_{bamo} \times (1 - e_{hawk})] \quad (1)$$

$$P_{dissipated,rear} = 30kW \times s_{rear} \times [(1 - e_{rinehart}) + e_{rinehart} \times (1 - e_{emrax})] \quad (2)$$

Assuming that all inefficiencies dissipate as heat, the MY19 cooling system will be required to dissipate 3.6 kW.

3.2 COOLING SYSTEM EQUATIONS

To determine the architecture of the cooling loop, an iterative model to solve for the flowrate given pressure drop was created.

The pressure drop across a pipe can be calculated by summing the major losses, minor losses and the pressure drop of large components, all in terms of flow velocity.

$$\Delta P = \Delta P_{major}(v) + \Delta P_{minor}(v) + \Delta P_{components}(v) \quad (3)$$

To calculate major losses, the Reynold's number (Re) and the Darcy friction factor (f) have to be calculated for a given flow velocity (v). Parameters required are the density (ρ) and dynamic viscosity (μ) of water, tube diameter (D) and roughness (ε).

$$\Delta P_{major}(v) = \sum f \frac{L}{D} \frac{\rho v^2}{2} \quad (4)$$

$$f = \left[-1.8\log\left(\frac{6.9}{Re} + \left(\frac{\frac{\varepsilon}{D}}{3.7}\right)^{1.11}\right)\right]^{-2} \quad (5)$$

$$Re = \frac{\rho v D}{\mu} \quad (6)$$

Minor losses can also be found given the minor loss coefficients ($K\ factors$), as shown in Table 2.

$$\Delta P_{minor}(v) = \sum K \frac{\rho v^2}{2} \quad (7)$$

Table 2: Minor loss coefficients (K factors) referenced from [1].

Type	K factor
45° Bend	0.4
90° Bend	1.5
T branch inline	0.9
T branch 90° bend	2

3.3 PRESSURE DROP TESTING

The pressure drop functions of the large components had to be found empirically. This was achieved with the help of a custom cooling test bench. The cooling test bench has a 5 gallon tank, with a heating element equipped with a temperature controller. A flowmeter is installed in the loop to measure the flowrate the pump is operating at. Components can be connected to it using quick-disconnect fittings. Each end of the quick-disconnects have temperature sensors and pressure gauges, so that temperature drop and pressure drop can be recorded across components. Figures 5 and 6 show the block diagram and the setup of cooling test bench.

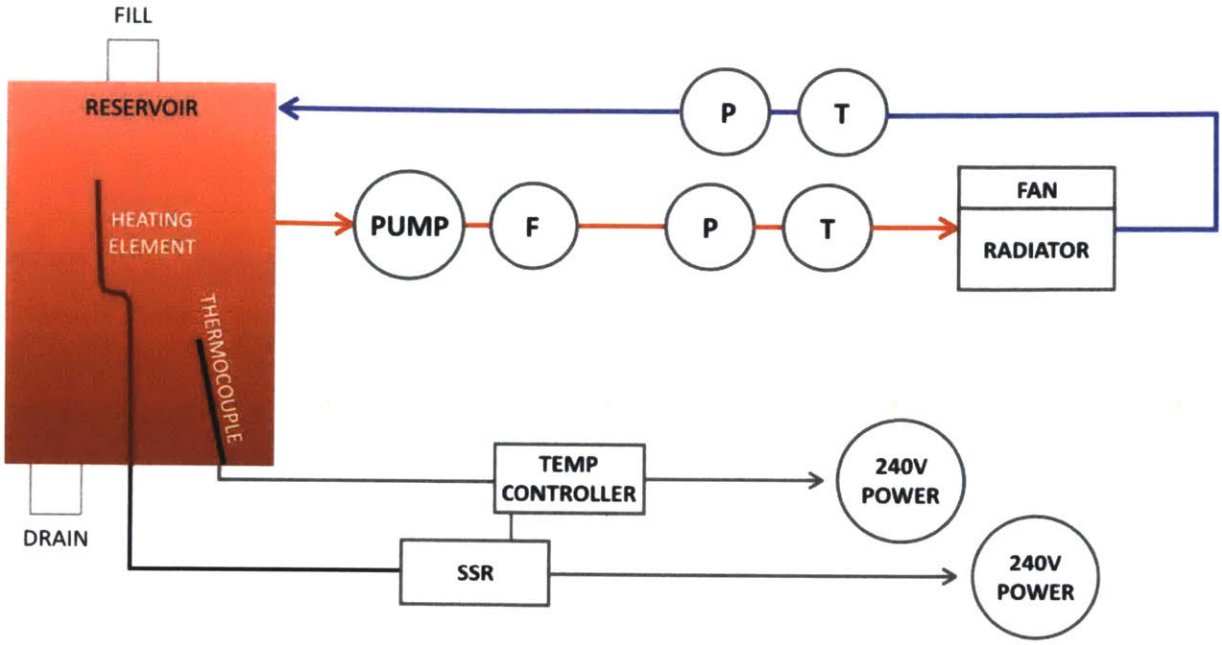

Figure 5: Block diagram of cooling test bench. Pressure sensors (P), temperature sensors (T), and a flowmeter (F) are positioned before and after the radiator to monitor performance.

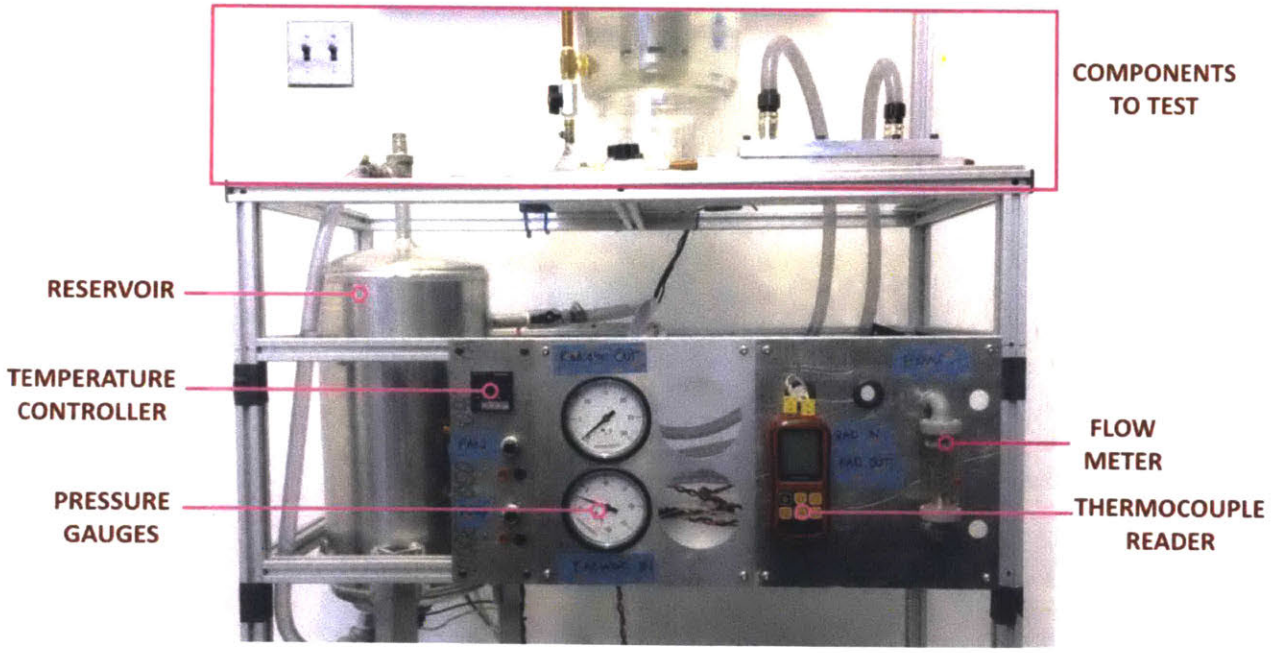

Figure 6: Cooling test bench setup.

The Rinehart, Emrax and Hawk 40 motors were connected to the test bench, and their pressure drops were recorded over a range of 3 to 11 liters per minute (LPM). For zeroing purposes, the pressure drop of the cooling bench system, and the 1/2in to 3/8in fitting adapters were recorded as well.

The pressure drop (ΔP) versus flowrate (Q) curves were fit to a quadratic form of $\Delta P = AQ^2 + BQ$. The data and their curve fits are shown in Figure 7. The Hawk 40 had the highest pressure drop while the Rinehart had the lowest pressure drop.

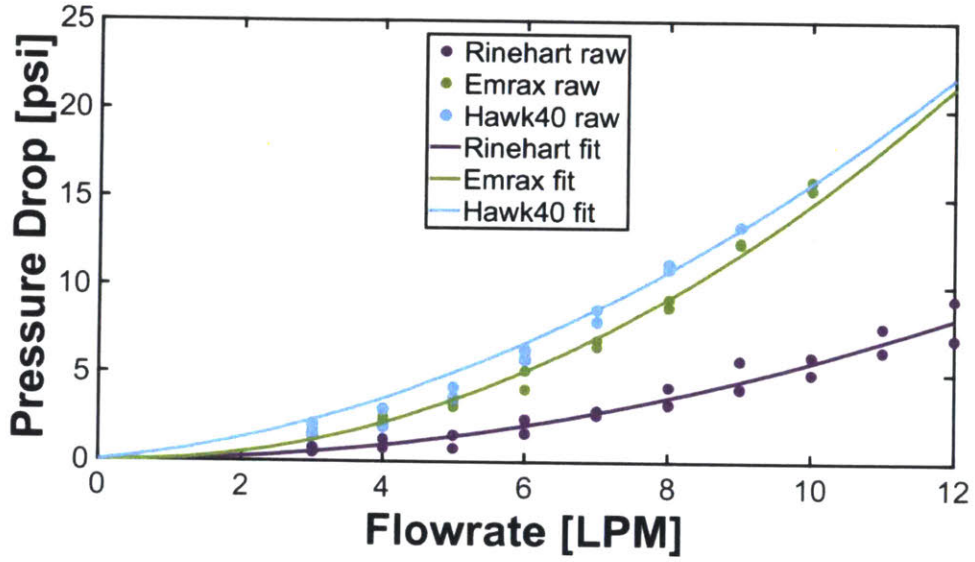

Figure 7: Pressure drop of Rinehart, Emrax and Hawk 40 motors with varying flowrates. All curves fit a quadratic form with an intercept at zero.

3.4 ARCHITECTURE

Knowing the pressure drop across the tube, components and fittings, different configurations of the cooling loop could be modelled. The process of iteration is as follows:

1. Determine which components to place in each branch
2. Vary total pressure drop across the branch
3. Use Excel Goal Seek to solve for flow velocity and flowrate given a tube diameter of 3/8in
4. Adjust the pressure drop such that the flowrate would be 7 to 8 LPM
5. Check if the pressure drop is reasonable for the pumps on the market.

The resulting architecture is as presented in Figure 8. The results from the iterative flowrate-pressure drop calculation are shown in Table 3.

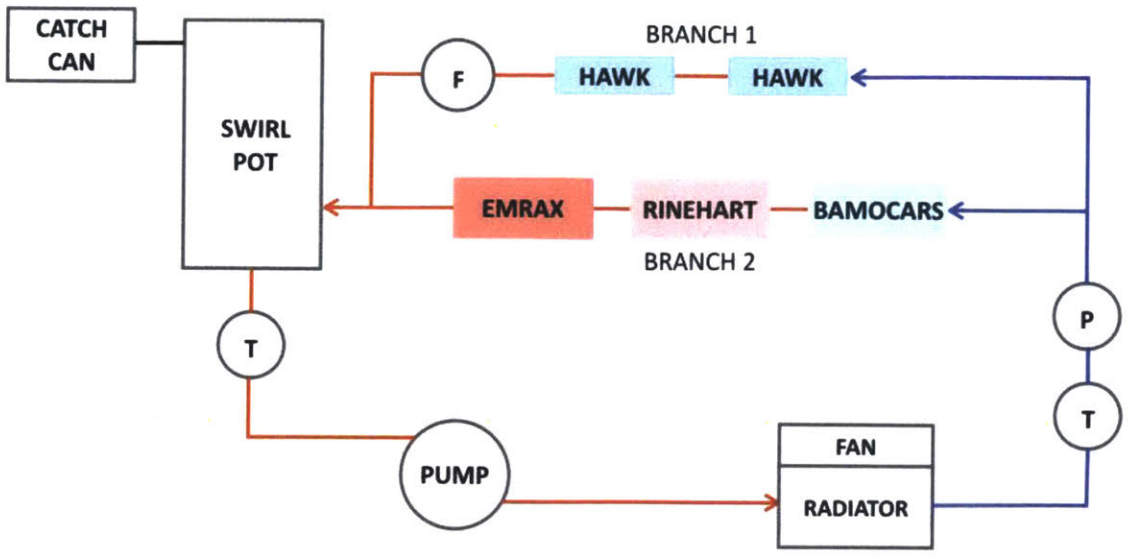

Figure 8: Parallel flow architecture with two Hawks in branch 1; Bamocars, Rinehart and Emrax in branch 2. Pressure sensors (P), temperature sensors (T), and flowmeter (F) can be integrated in the loop to monitor performance.

Table 3: Results from iterative flowrate-pressure drop calculation. Total flowrate is about 15 LPM and pressure drop across branches is about 30 psi.

	Velocity iterated [m/s]	ΔP [N/m^2]	Q [m^3/s]	Q [LPM]
Branch 1	**1.88**	200000	1.34E-04	8.06
Branch 2	**1.83**	200000	1.31E-04	7.84
Total			2.65E-04	15.89

The two Hawk 40s are in branch 1, while all other components are in branch 2. This is beneficial for routing as the front motors are in their own loop and can minimize tubing. The motor controllers are placed first in the branch 2, as they are more sensitive to temperature spikes. The pressure drop across the entire cooling loop including the radiator and fittings is about 40 psi.

3.5 COOLING COMPONENTS

PUMP

On MY18, the cooling system used a diaphragm water pump, which although heavy, reliably provided adequate flowrate for the given pressure drop. For MY19, the goal was to reduce the mass without compromising performance.

Centrifugal and diaphragm pumps were considered for MY19. A centrifugal pump has a rotating impeller that accelerates the fluid. The fluid exits the pump at a higher velocity due to centrifugal force. A

centrifugal pump cannot be run dry and needs to be primed. A diaphragm pump is a positive displacement pump that uses expanding and contracting cavities to push the fluid. Unlike a centrifugal pump, a diaphragm pump can maintain constant flowrate at any discharge pressure. A diaphragm pump can further be run dry without damage. These benefits of a diaphragm pump led to the decision to use one for MY19.

Off the shelf diaphragm pumps were able to meet my pressure head requirement of 40 psi at 15 LPM. However, these pumps have large brushed DC motors that contribute the majority of its heavy mass. Before a lower mass solution was found, a temporary pump, Everflo Diaphragm Pump Model EF7000, was chosen for the cooling system, and is shown in Figure 9.

Figure 9: Everflo Diaphragm Pump Model EF7000. At no load it can operate at 7.0 GPM (26.7 LPM). It weighs 4.3 kg.

With no lighter diaphragm pumps on the market, in-house modification was required. A pump was disassembled, and its heavy brushed motor was replaced with a lighter brushless motor. The brushless motor used can provide maximum of 744 W of power, which provides a large margin for the 69 W power requirement from pressure drop and flowrate. However, the efficiency, torque and speed requirements of the pump could not be determined, so testing was needed to determine whether the motor was appropriate. The shaft in the brushless motor was replaced to match the coupling in the diaphragm. Figure 10 shows the brushless motor pump prototype.

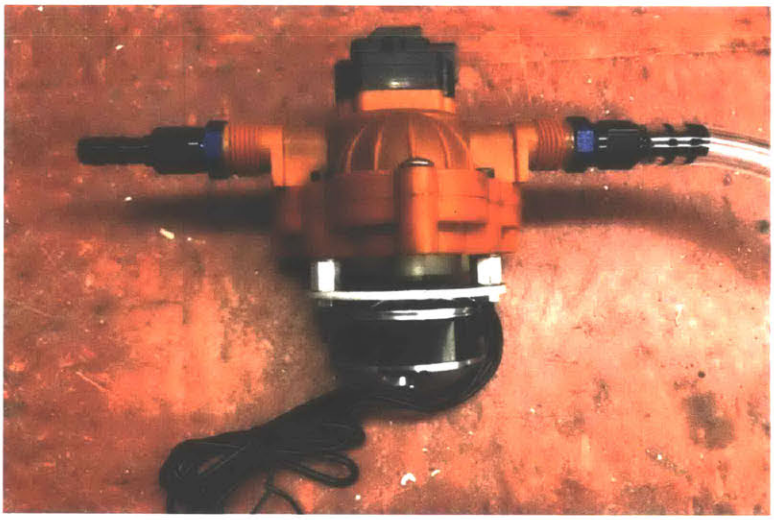

Figure 10: The prototype pump, nicknamed "Frankenpump", with T-motor model MN5212 KV340.

The prototype was connected to a flowmeter, and it could achieve 11 LPM of flow with the motor at its maximum capacity, drawing about 120 W. Figure 11a and 11b show the testing set up and resulting flowrate.

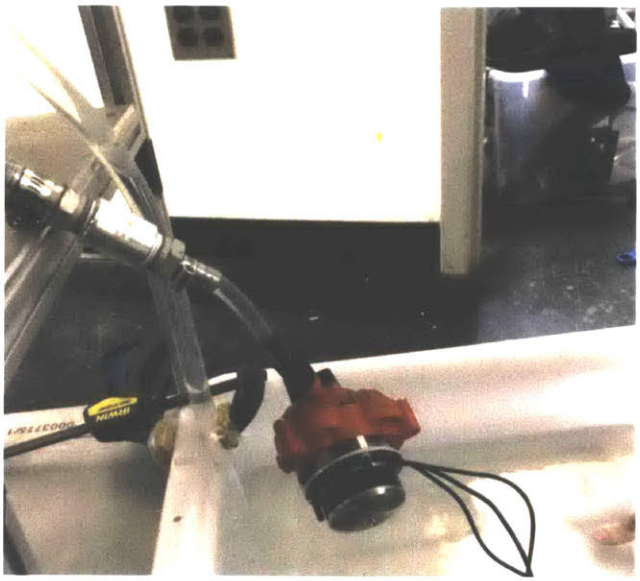

Figure 11a and 11b: Frankenpump flowrate test setup and flowmeter showing the flowrate of 11 LPM.

To reach a flowrate of 15 LPM, the next step is to replace the KV340 brushless motor with the KV420 model, which has a maximum power of 1440 W and maximum RPM of 7440.

There is risk of mechanical failure in the diaphragm pump head, as it may not be designed to operate at high speeds. These risks will be mitigated through testing and inspecting for signs of wear. If this pump head fails, a more robust diaphragm pump head can be used.

RADIATOR AND FAN

To push enough air through the radiator, an appropriate fan has to be selected. Analytically, the airflow across the radiator can be modelled to obtain the pressure drop across the radiator, and can be plotted against the fan curve to estimate the operating point of the fan.

Pressure drop across the radiator can be modelled as sudden contraction as the air enters the fins, major losses as air travels through the fins and sudden expansion as air exits the radiator. Knowing the length (L) and width (W) of the radiator, the total area where the air enters (A_{in}) the radiator can be found.

$$A_{in} = L \cdot W \tag{8}$$

The area of airflow through each fin channel ($A_{channel}$) can be measured and total area (A_{out}) can be estimated by counting the number of channels on the radiator ($N_{channel}$).

$$A_{out} = A_{channel} \cdot N_{channel} \tag{9}$$

Given a range of flowrates (Q), the flow velocity (v_{pipe}) through the fin channels of the radiator can be calculated.

$$v_{pipe} = \frac{Q}{A_{in}} \cdot \frac{A_{in}}{A_{out}} \tag{10}$$

Pressure drop from contraction and expansion can be calculated from the equations 11 and 12.

$$\Delta P_{contract}(v_{pipe}) = \frac{1}{2}\rho_{air}(v_{pipe})^2 \left(\frac{A_{out}}{A_{in}} - 1\right)^2 \tag{11}$$

$$\Delta P_{expand}(v_{pipe}) = -\frac{1}{2}\rho_{air} \cdot \frac{A_{out}}{A_{in}}\left(1 - \frac{A_{out}}{A_{in}}\right) {v_{pipe}}^2 \tag{12}$$

Pressure drop from major losses can be calculated using equations 4, 5, and 6. For diameter (D), hydraulic diameter (D_h) was used due to the irregular shape of the fin channels. The perimeter of the channels ($P_{channel}$) was found through measurement.

$$D_h = \frac{4 \cdot A_{channel}}{P_{channel}} \tag{13}$$

The total pressure drop across the radiator is the sum of the calculated pressure drops above.

$$\Delta P = \Delta P_{contract} + \Delta P_{major} + \Delta P_{expand} \tag{14}$$

Figure 12 shows the total pressure drop across a Yamaha YFM700R raptor aluminum radiator that was used on MY19.

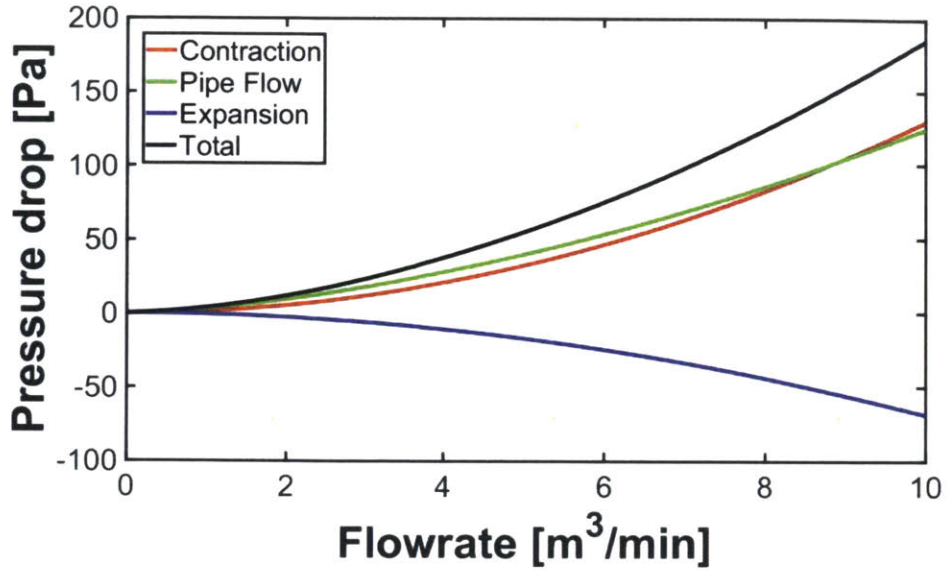

Figure 12: Total pressure drop across a Yamaha YFM700R raptor aluminum radiator. Pipe flow and contraction dominate the pressure drop.

Fan curves were then plotted together with the total pressure drop determined from the radiator model, as shown in Figure 13. These fan curves were obtained from manufacturer datasheets [6],[7],[8],[9]. A range of fans were considered, including SPAL brand fans that are used in racing, and computer fans from Sanyo Denki.

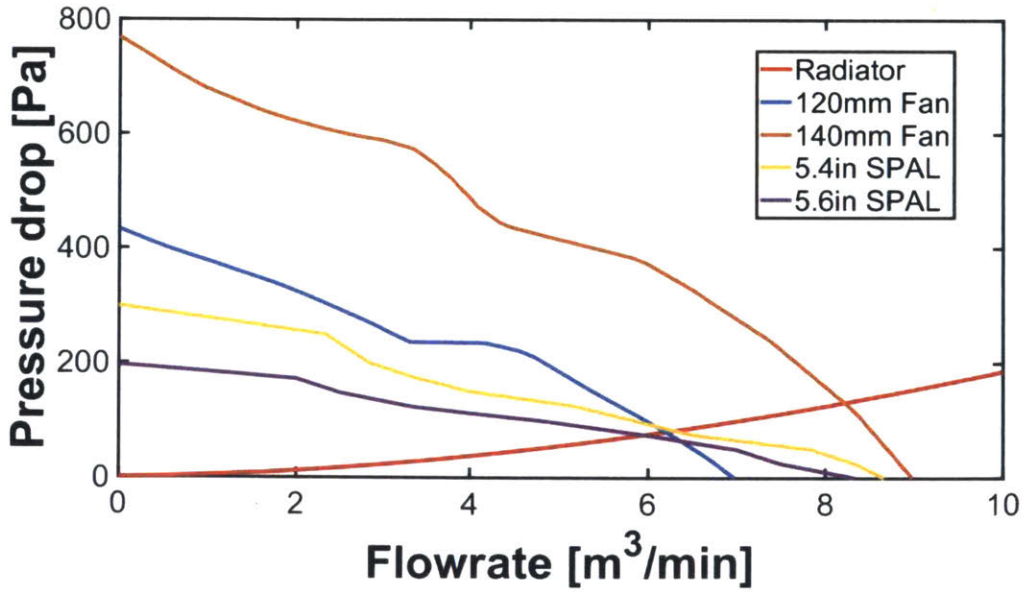

Figure 13: Fan curves from a 120mm and 140mm Sanyo Denki fans and 5.4in and 5.6 SPAL fans and the total radiator pressure drop. The 120mm, 5.4 in and 5.6in fans had operating points at around 6 to 7 $\frac{m^3}{min}$.

Since this pressure drop is purely analytical, further testing is required to determine fan performance. The 120mm and 140mm fans from Sanyo Denki were purchased for further testing, as they are lighter than the SPAL fans of comparable size.

An aluminum Mishimoto dirt bike radiator larger than the one on MY18 was modified with Earls fittings and tabs. A larger radiator was purchased for comparison purposes. The fan was connected to the radiator by an aluminum shroud fitted with PEM inserts, shown in Figure 14.

Figure 14: Radiator and fan shroud assembly.

SWIRL POT

Once the flow goes through the motors and motor controllers, the branches merge and water enters the swirl pot. The swirl pot, shown in Figure 15, aims to reduce flow velocity through the diffuser, allows air to escape through vortexing and avoids introducing more air as the water leaves through the outlet.

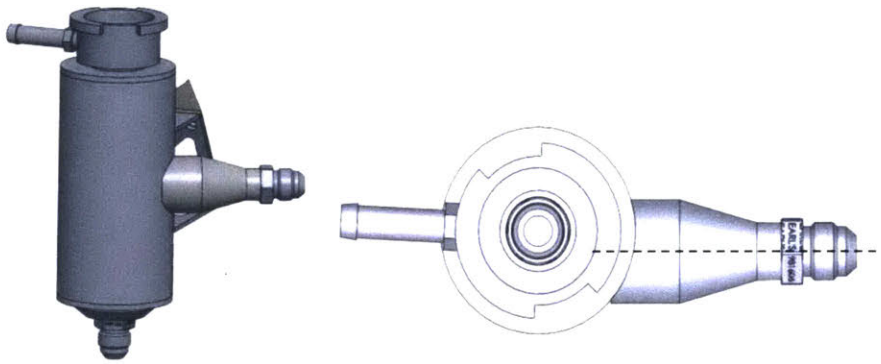

Figure 15a and 15b: The inlet on the left leads water into the diffuser, and the water vortexes down to the outlet which connects to the pump. The inlet is offset from the center plane so that the flow can vortex down the cylinder.

The diffuser has a higher surface roughness to introduce turbulence such that air can escape. The fill neck at the top has a cap that is rated for 19 psi. If the pressure rises above 19 psi, fluid flows out into a catch can.

Flow simulations were attempted to determine where to place the fluid inlet – high up, midway or lower closer to the outlet. An inlet mass flow is applied, and the bottom outlet has the boundary condition of environmental pressure. Gravity is also modelled. The resulting flow trajectories are seen in Figure 16.

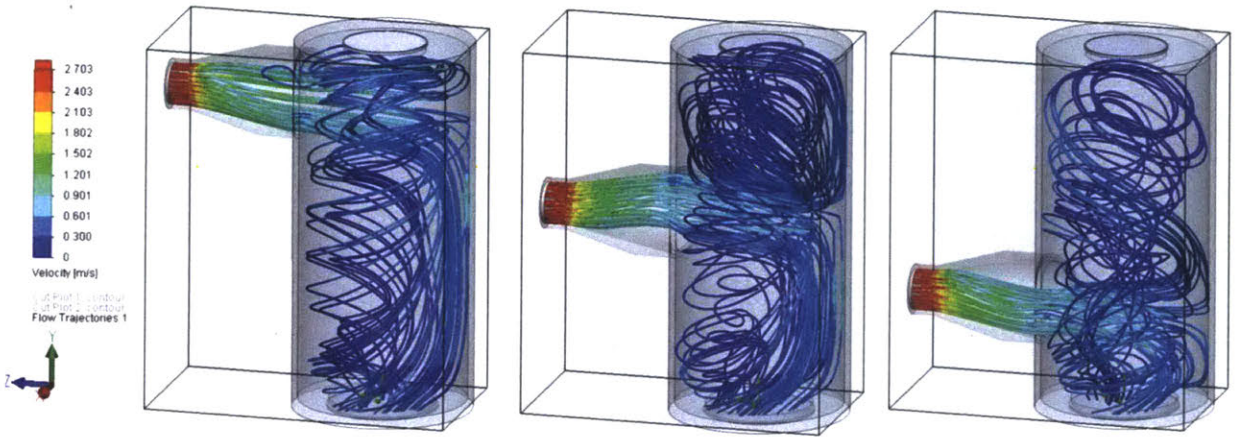

Figure 16: Solidworks Flow Simulation flow trajectory plots predict how water will vortex depending on the location of the fluid inlet.

It was difficult to interpret the behavior of cavitation in the flow simulation, so the design was chosen intuitively. The diffuser was placed in the middle configuration, so that water will be less likely to spill out the fill neck but still allow for sufficient swirling.

CAD

Full system CAD and routing was integrated into the car CAD. Figure 17 shows the cooling system components with the front and rear powertrain.

Figure 17: CAD of cooling system on frame with front and rear powertrain.

4. SYSTEM PERFORMANCE

The radiator and fan from MY18 was placed on the cooling test bench to evaluate the amount of heat dissipated. Temperature readings were taken at the inlet (T_{in}) and outlet (T_{out}) of the radiator at varying flowrates ($\dot{m}$), with the fan operation at its maximum speed. Figure 18 shows the experimental setup.

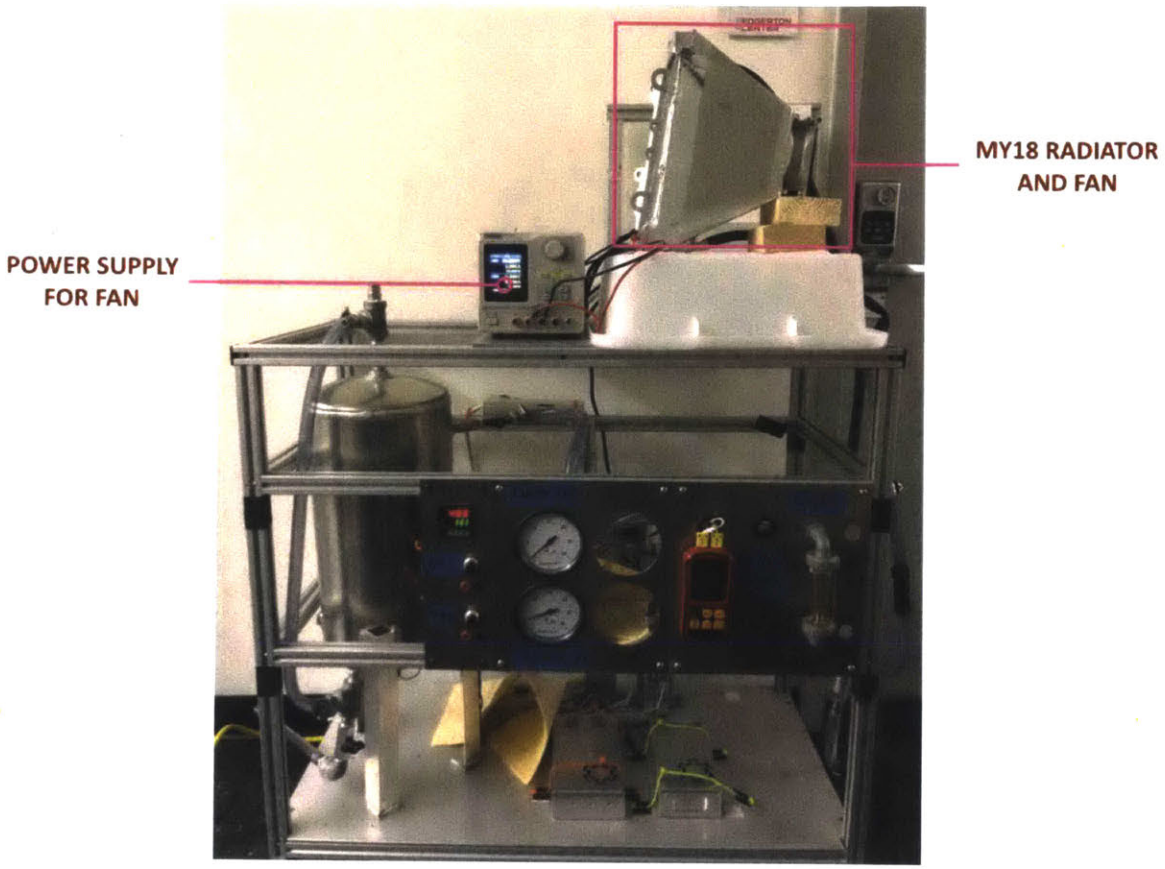

Figure 18: MY18 radiator and fan setup on the cooling test bench to measure temperature drop across the radiator

Heat dissipation was calculated using equation 15, using the specific heat capacity of water (c_p) at the average water temperature.

$$\dot{Q} = \dot{m} c_p (T_{in} - T_{out}) \quad (15)$$

The larger radiator and fans chosen for MY19 were also tested. Figure 19 shows the heat dissipated by MY18's radiator and fan, and the MY19 radiator with the stronger as 140mm fan, and with weaker 120mm fan.

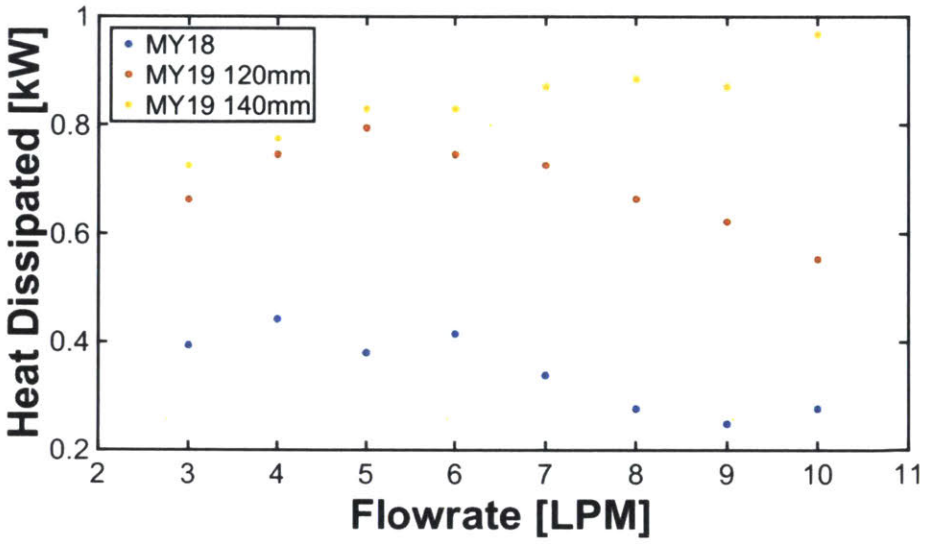

Figure 19: Heat dissipation of various radiators and fans at different flowrates. Heat dissipation across different flowrates is mostly consistent within $\pm 0.1\ kW$.

According to the tests, the MY18 system dissipated about 0.35 kW of heat. This is an order of magnitude less than the estimated 3.2 kW of inefficiency calculated from the 30 kW of average power draw. The discrepancy may be attributed to the thermal mass of the components.

With a larger radiator and larger fan, the MY19 system can double the heat dissipated at about 0.7 kW. Since the 3.2 kW estimated inefficiency for MY18 was inaccurate, it is difficult to predict how much heat MY19 will dissipate through its powertrain.

5. CONCLUSIONS AND FUTURE WORK

The MY19 cooling system was designed from the ground up, by determining flow architecture and component requirements through modelling and testing. It has yet to be proven to meet its functional requirements due to the fact that the front powertrain has not been integrated on the car. Once the front powertrain has been connected to the cooling loop, performance will be optimized through the use of pressure and temperature sensors. A flowmeter can also be included to monitor flowrate.

APPENDIX

Relevant FSAE rules for cooling [10]

T.7.3 Coolant Fluid

T.7.3.1 Water cooled engines must use only plain water with no additives of any kind.

T.7.3.2 Electric motors, accumulators or HV electronics may use plain water with no additives or oil as the coolant.

T.7.4 System Sealing

T.7.4.1 Any cooling or lubrication system must be sealed to prevent leakage.

T.7.4.2 The vehicle must be capable of being tilted to a 45° angle without leaking fluid of any type.

T.7.5 Catch Cans

T.7.5.2 Any vent on other systems containing liquid lubricant or coolant, including a differential, gearbox, or electric motor, must have a catch can with a minimum volume of 10% of the fluid being contained or 0.5 liter, whichever is greater.

T.7.5.3 Catch cans must be:

a. Capable of containing boiling water without deformation

b. Located rearwards of the firewall below the driver's shoulder level

c. Positively retained, using no tie wraps or tape

T.7.5.4 Any catch can on the cooling system must vent through a hose with a minimum internal diameter of 3 mm down to the bottom levels of the Frame.

T.3.5 Firewall

T.3.5.1 A firewall must separate the driver compartment from all components of the fuel supply, the engine oil, the liquid cooling systems, any lithium batteries and any high voltage system.

REFERENCES

[1] RMS PM/RM Hardware User Manual Revision 3.0. <app.box.com/s/vf9259qlaadhzxqiqrt5cco8xpsn84hk/file/23982227247>.

[2] User's Manual for Advanced Axial Flux Synchronous Motors and Generators. <emrax.com/wp-content/uploads/2017/01/user_manual_for_emrax_motors_january_2017_version_4.5.pdf>.

[3] MANUAL Digital Three-Phase Servo Amplifier BAMOCAR-PG-D3. <www.unitek-industrie-elektronik.de/images/pdf/BAMOCAR%20Digital/BAMOCAR-PG-D3_EN.pdf>.

[4] Hawk40 210V Installation Manual Revision 1.3. 2018.

[5] White, Frank Mangrom., and Rhim Yoon. Chul. Fluid Mechanics. 8th ed., McGraw-Hill Education, 2016.

[6] San Ace 120 9GV type. <https://www.mouser.com/datasheet/2/471/San_Ace_120GV38_E-1282430.pdf>.

[7] San Ace 140 9WL type. <https://www.mouser.com/datasheet/2/471/San_Ace_140WL51_E-1370594.pdf>.

[8] SPAL Automotive VA31-A101-46S. <https://webstore.spalusa.com/content/files/content/PDF/30103013_SPEC.pdf>.

[9] SPAL Automotive VA32-A101-62S. <https://webstore.spalusa.com/content/files/content/PDF/30103009_SPEC.pdf>.

[10] Formula SAE Rules 2019 <https://www.fsaeonline.com/cdsweb/gen/DownloadDocument.aspx?DocumentID=64b861c2-980a-40fc-aa88-6a80c43a8540>.